Spring 2021

# Cold Plasma Enhanced Active Sites on Supported NiP Nanoparticles for the Oxygen Evolution Reaction

Michael Ricci
mjr150@zips.uakron.edu

# Cold Plasma Enhanced Active Sites on Supported NiP Nanoparticles for the Oxygen Evolution Reaction

Honors Project Report
Department of Chemical Engineering
The University of Akron


Advisor: Dr. Zhenmeng Peng

Author: Michael Ricci

Course: 4200:497-001

Date: April 23, 2021

# Contents

## Executive Summary

Global energy demands continually grow and are met by relying on non-renewable fossil fuels which are large contributors to climate change. Water electrolysis provides a unique route to convert intermittent, clean renewable energy into chemical energy by electrochemically splitting water into oxygen and hydrogen gases, the latter of which can be stored and converted back into electricity without any cost to the environment. Identifying materials to efficiently catalyze the naturally sluggish oxygen evolution reaction (OER) is key to increasing efficiency in water electrolyzers, giving resolution towards achieving a sustainable energy future.

Several electrocatalysts have been identified to demonstrate acceptable OER activity, however few materials that are both highly active and earth-abundant have been identified. Nickel phosphide (NiP) can be synthesized from common materials and is a somewhat active electrocatalyst for OER. During OER, the surface of transition metal based electrocatalysts are partially oxidized and occupy mixed-valence oxidation states, which have been identified as the active sites for OER. Cold plasma treatment subjects materials to an environment of highly energetic ionic species which could be used to selectively control the oxidation state of surface active sites, in this case, on OER electrocatalysts. In this work, NiP nanoparticles were synthesized on an activated carbon support (NiP/C) using a solid-state method and were then treated in oxygen, hydrogen, and argon plasmas for varying times in an effort to enhance the activity of the material.

OER activity of the samples produced through the various treatments was evaluated by testing the materials in alkaline conditions (1M KOH). The activities of the treated samples were normalized by the number of active sites, estimated by the area under the $Ni^{2+}/Ni^{3+}$ oxidation

peak, providing the intrinsic activity characteristic of the surface of the material, and a more direct activity comparison between samples. A short 1-minute treatment in argon plasma yielded the greatest improvement, an approximate 19% increase in intrinsic activity (544 A/mmol) compared to the untreated NiP/C (456 A/mmol). Treatments in dilute 5% $O_2$ (in Ar) and 1% $H_2$ (in Ar) did not significantly benefit the OER activity of the catalyst.

In all cases, plasma treatment reduced the number of active sites on the support as measured through electrochemical methods. The plasma atmosphere likely sputtered catalyst from the carbon support during treatment, physically reducing the number of active sites. Although the intrinsic activity of the material was seen to improve after plasma treatment, the reduction in the number of active sites translates to a decreased mass activity. As such, the overall performance of the electrodes prepared with 1-minute argon plasma treated was similar to the performance of electrodes prepared with untreated material.

XPS analysis was used to identify any correlation between the improvement seen in the intrinsic activity of the material and the oxidation state of chemical species on the surface of the material after plasma treatment. While changes in oxidation state after plasma treatment are obvious from the XPS data, no meaningful correlation could be established.

Through this work, plasma treatment has been tested and proven as a quick and facile method to alter the surface chemistry of carbon supported NiP. Future paths could explore optimizing treatment conditions to provide a milder condition that preserves active sites on the bulk material while achieving the desired control over active site valency. For OER applications, electrocatalysts derived from transition metals with lower redox potentials could be treated and evaluated in a similar manner to provide a correlation between valence and OER activity which can be more easily observed.

# Introduction

As the global energy demand grows, it continues to be met by an energy infrastructure constructed around a finite supply of fossil fuels.[1-3] Risks of climate change associated with the consumption of carbon-based fuels provide further incentive for a reconstruction of the current chemical and energy infrastructure, to shift dependence from oil, gas, and coal supplies to renewable sources.[1-4] Hydrogen has attracted much attention as an alternative fuel because it can be produced sustainably through water electrolysis using renewable energy, then cleanly converted back to electrical energy through its oxidation to water in fuel cells.[1-3, 5-7]

Of the available electrochemical methods for water splitting, alkaline water electrolysis is one of the most straightforward with the added benefit of the ability to utilize earth abundant metal catalysts to split water at low temperatures.[6, 8-9, 11] Reducing the large overpotential barrier of the anodic oxygen evolution reaction (OER) remains as one of the biggest challenges preventing improved water electrolysis efficiency and continues to be an active area of electrocatalysis research.[7, 9, 11-18]

The most active electrocatalysts for OER are noble metal oxides, namely ruthenium oxide and iridium oxide, but are costly, in limited supply, and have poor durability in alkaline environments.[11-12] Transition metal phosphides, particularly NiP, have been studied as effective catalysts for alkaline OER due to their increased performance, compared to transition metal oxides, attributed to higher intrinsic conductivity.[7, 10-13, 18]

During electrolysis, the surface of transition metal based electrocatalysts undergo phase change resulting in multivalent oxidation states, which have been identified as the active sites for OER.[7, 12] Several efforts in materials and surface engineering have focused on tuning catalyst

materials to gain control over the valence of surface active sites on transition metal catalysts. Cheung, et al. have synthesized a composite $IrO_x$-$TiO_2$-Ti catalyst with unique mixed-valence states of surface $IrO_x$ with improved OER activity.[14] It was demonstrated by Zhang, et al. that incorporating high valence metal modulators in metal compounds benefits OER activity through the optimization of Ni, Co, and Fe site oxidation cycles.[15] Several other studies have focused on surface engineering of perovskites through annealing and post-treatment with oxidative and reductive chemical methods demonstrating that the valence of transition metals in these materials can be controlled after synthesis to improve the OER activity.[16, 17]

Cold, non-equilibrium plasmas produced through dielectric barrier discharge (DBD) provide a novel opportunity to tune the surface chemistry of catalyst materials without the use of high temperature or chemical based approaches. Plasma approaches in material synthesis and treatment are advantageous over thermal treatment methods in that sintering is avoided and materials are treated in a matter of minutes rather than hours.[19-21] Plasma has been used by Wirth, et al. to treat carbon support leading to improved catalyst dispersion over the support and enhance activity of the oxygen reduction reaction.[22] The plasma atmosphere of excited ions, radicals, and electrons can also alter the molecular structure and valence of catalyst active sites depending on factors such as the plasma species and treatment time.[20]

In this work, we explore plasma treatment as a facile method to control the valence state of Ni active sites on NiP nanoparticles. Conditions under different atmospheres and varying treatment times were considered to optimize the OER activity of the catalyst.

# Experimental Methods

## Reagents

Vulcan XC72 carbon black (Cabot), nickel(II) nitrate hexahydrate ($Ni(NO_3)_2 \cdot 6H_2O$, 98%, Alfa Aesar), sodium hypophosphite monohydrate ($NaH_2PO_2 \cdot H_2O$, Alfa Aesar), and ethanol (200 proof, Decon Laboratories, Inc.) were used as received for NiP/C synthesis. High purity Ar, 5% $O_2$ in Ar, $H_2$, and $O_2$ (all from Praxair) were used for plasma treatment and electrochemical experiments.

## Material Preparation

NiP/C was prepared following a solid-state synthesis route similar to that detailed by Guan, et al.[23] $Ni(NO_3)_2 \cdot 6H_2O$ precursor was dissolved in ethanol and loaded onto the activated carbon support. Targeting a 20 wt% Ni loading, 0.5 g of $Ni(NO_3)_2 \cdot 6H_2O$ precursor was dissolved in 2 mL ethanol and loaded dropwise onto 0.5 g of activated carbon then dried at 80°C overnight.

Two ceramic tube furnace boats were prepared by placing 0.1 g of $NaH_2PO_2 \cdot H_2O$ behind 0.1 g of the precursor on carbon support to achieve a 1:5 Ni:P molar ratio for synthesis. The boats were arranged in the middle of a tube furnace such that the $NaH_2PO_2 \cdot H_2O$ was upstream of the catalyst powder. After purging the furnace for 20 min with Ar, the materials were heated to 400°C at a rate of 10°C/min and held at 400°C for 2 hrs under 75 sccm Ar flow. After sufficient cooling, the NiP/C was washed twice with water and centrifuged at 4500 rpm for 30 min, then dried at 80°C overnight. Several batches were synthesized and combined to produce a large sample of bulk material for treatment and testing.

## Plasma Treatment

**Table 1:** Summary of samples evaluated for OER performance with treatment details

| Gas | % in Argon | Treatment Time (min) | Samples Treated/Tested |
|---|---|---|---|
| Untreated | - | - | 3 |
| Oxygen | 5 | 5 | 2 |
| | | 3 | 2 |
| | | 1 | 3 |
| Hydrogen | 1 | 1 | 3 |
| Argon | - | 1 | 3 |

An in-house DBD plasma reactor was carefully loaded with 20 mg of as prepared NiP to ensure the material was distributed uniformly in a thin layer along the bottom of the reactor and within the active plasma region. The reactor was purged with the desired gas (combination) for 15 minutes prior to treatment. The plasma drive was set to output 90W, providing a mild plasma atmosphere. The gas flow rate for all samples was 100 mL/min during purging and treatment. Treatment conditions tested are detailed in **Table 1**. For treatment times longer than 1 minute, the total treatment time was divided into two successive treatments and the reactor was allowed to cool after the first. The oxygen atmosphere was provided by a premixed gas consisting of 5% oxygen in argon. Other plasma atmospheres were provided by diluting the desired gas with argon via flow control.

## Electrode Preparation

Catalyst inks (2 mg catalyst/mL) were prepared by dispersing an appropriate amount of catalyst (e.g. NiP/C) in an IPA/water solution ($V_{IPA} = V_{H2O}$) under 30 min ultrasonication with Nafion ionomer added as a binder (4 µL Nafion/mg catalyst). 19.6 µL of the catalyst ink was deposited dropwise onto a glassy carbon rotating disc electrode (GCE) (5 mm diameter) using an

in-house spin coating device at 350 rpm under gentle warm air flow. A thin film of catalyst was formed on the GCE, achieving a catalyst loading of 0.2 mg/cm$^2$.

## Electrochemical Measurements

A three-electrode cell was assembled with the prepared glassy carbon rotating disc electrode as working electrode, Ag/AgCl (1M KCl) reference electrode, and Pt wire counter electrode. All tests were performed at a rotation rate of 1500 rpm in 1M KOH, saturated with $O_2$ for 15 minutes prior to the experiment. A CH Instruments 760D electrochemical workstation was used as the potentiostat for electrochemical measurements of the three-electrode system.

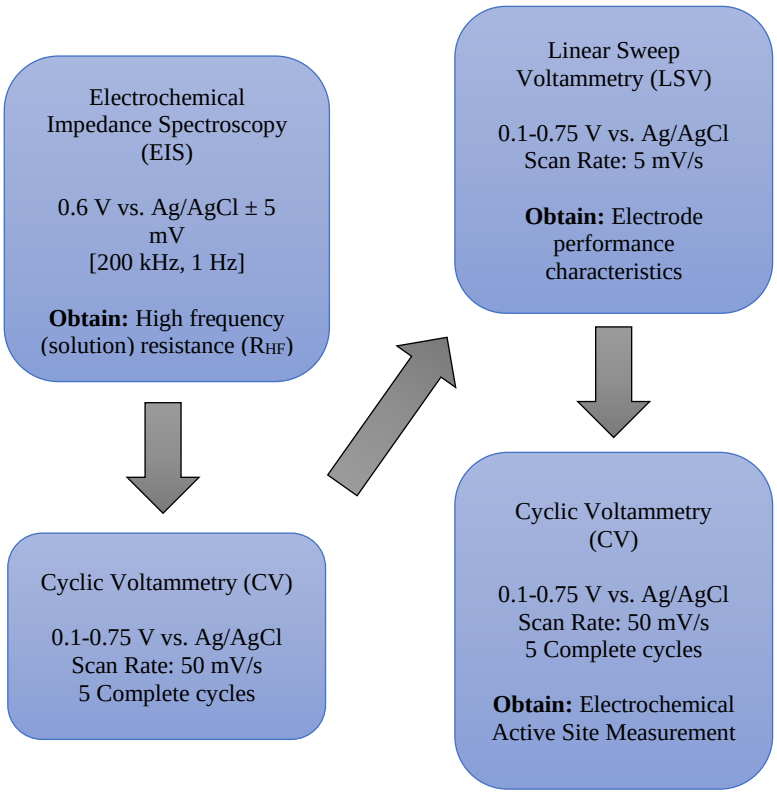


**Figure 1:** Electrochemical testing sequence used to evaluate electrode activity

The testing sequence (**Figure 1**) was designed to evaluate electrode performance in several steps. EIS was used to estimate the solution resistance ($R_{HF}$), the electrode was stabilized during 5 initial CV scans, an LSV curve was generated to obtain performance characteristics of the electrode (**Figure 2**), then 5 more CV scans were generated, the first of which was used to estimate the number of OER active sites on the electrode (**Figure 3**). For reporting purposes, the

potential recorded against Ag/AgCl ($E_{Ag/AgCl}$) was converted to potential versus the Normal Hydrogen Electrode ($E_{NHE}$) according to: $E_{NHE} = E_{Ag/AgCl} - iR_{HF} + 0.059\,pH + 0.228$, where 0.059 (V/pH) is the Nernst slope of the water redox reaction and 0.228 is the potential the reference electrode against NHE.

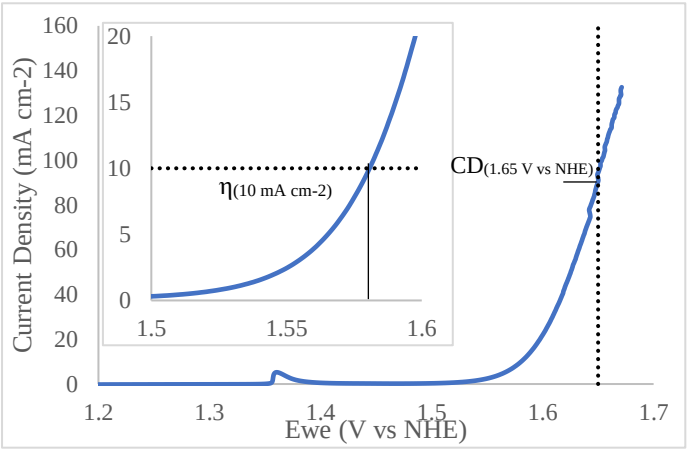


**Figure 2:** LSV curve of untreated NiP/C showing locations of overpotential and current used for performance comparisons.

The current density at 1.65 V vs NHE ($CD_{(1.65\ V\ vs\ NHE)}$) and overpotential at 10 mA $cm^{-2}$ ($\eta_{(10\ mA\ cm\text{-}2)}$) were used to compare performance between samples. Overpotential was calculated as the difference between the working electrode potential and the thermodynamic potential of the water redox reaction ($E^0$): $\eta_{(10\ mA\ cm-2)} = E_{NHE} - E^0 = E_{NHE} - 1.23$ .

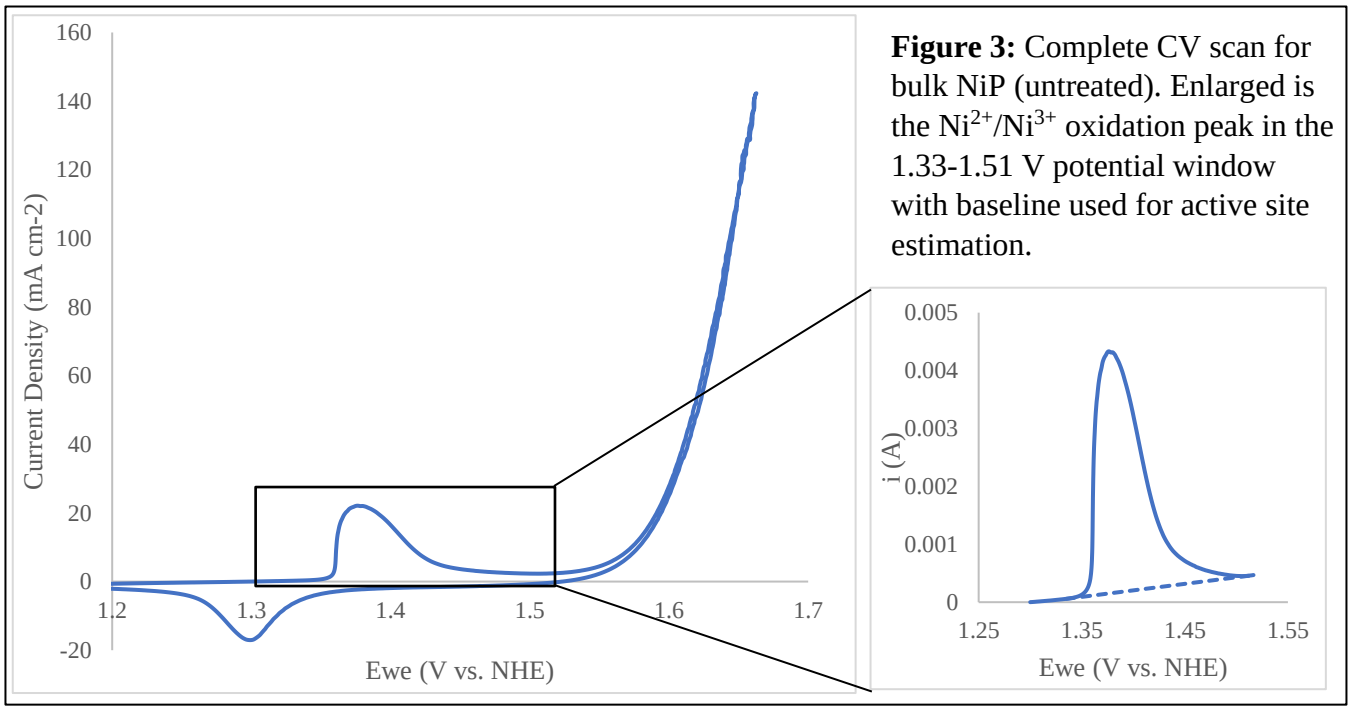


**Figure 3:** Complete CV scan for bulk NiP (untreated). Enlarged is the $Ni^{2+}/Ni^{3+}$ oxidation peak in the 1.33-1.51 V potential window with baseline used for active site estimation.

The number of active sites for each sample was estimated considering the area under the $Ni^{2+}/Ni^{3+}$ oxidation peak seen in the complete CV scan in the 1.33-1.51 V (vs. NHE) potential window (**Figure 3**). Integrating current with respect to voltage, the total charge of $Ni^{2+}/Ni^{3+}$ oxidation (Q) was determined according to $Q = \left(\frac{1}{S}\right) * \int_{1.33}^{1.51} i\, dV$, where S is the scan rate in V/s. Area under the sloped line background fitted to the data accounting for double-layer capacitive effects was subtracted from the charge after integration. The number of active sites was estimated by $n_{act} = n_{e-} = Q/F$, considering one mole of electrons is required to oxidize one mole of $Ni^{2+}$. It should be noted that the exact valence states of the material could vary from 2+/3+ during oxidation, however, this method should suffice for relative comparison between samples.

## Material Characterization

X-ray diffraction (XRD) characterization was carried out on a Bruker AXS Dimension D8 X-ray diffractometer with a Cu Kα radiation source. X-ray photoelectron spectroscopy (XPS) was conducted using a PHI VersaProbe II Scanning XPS Microscope under ultra-high vacuum. XPSPEAK peak fitting software was used to deconvolute the spectra. XPS spectra were not corrected to the adventitious carbon peak due to the uncertain nature of the carbon signals in the treated and untreated samples.[24] Transmission electron microscopy (TEM) images were captured using a JEOL JEM-1230 microscope operated at 120 kV.

# Results and Discussion

## Material Characterization

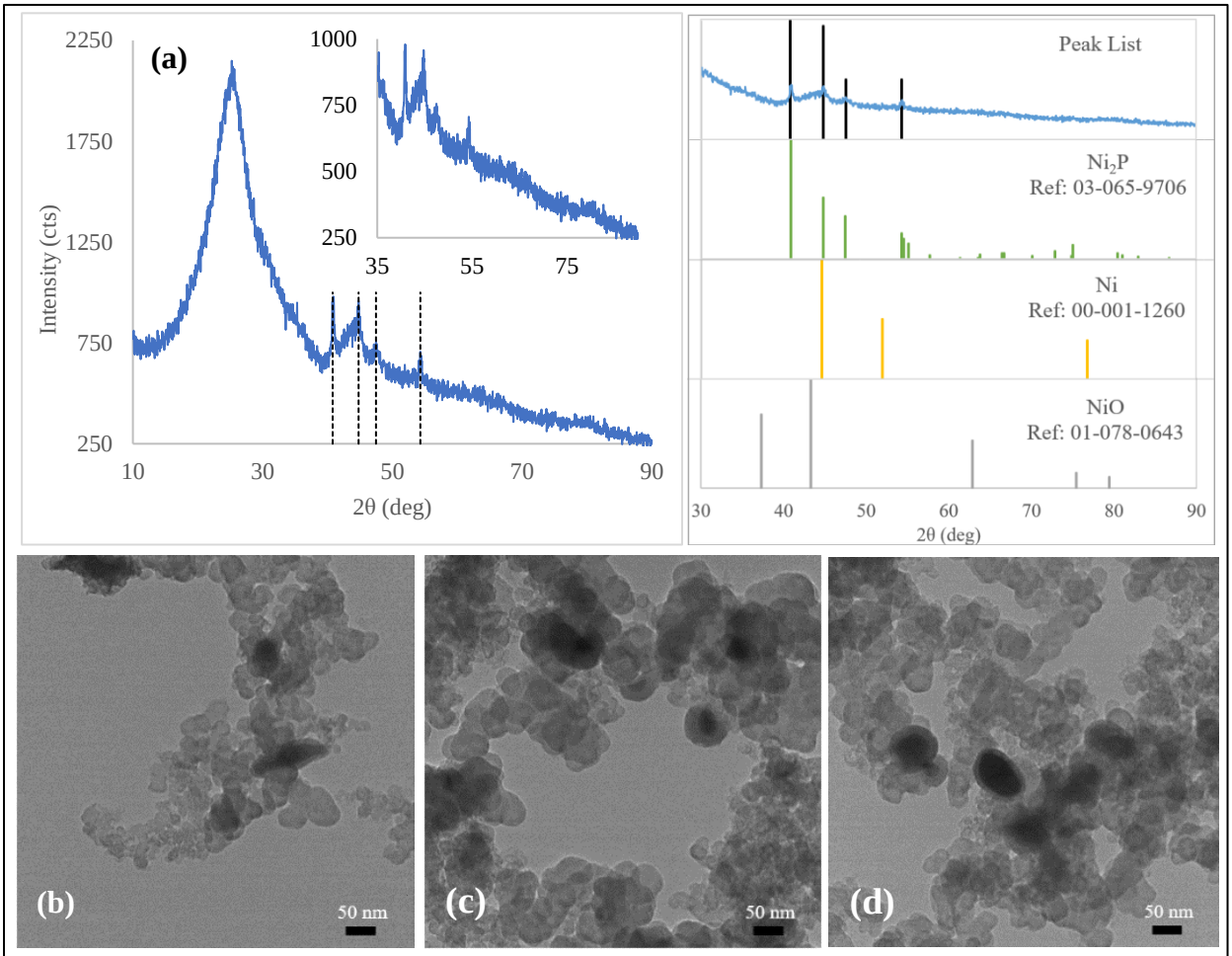


**Figure 4: (a)** XRD pattern of as prepared bulk NiP/C, with peak list and reference patterns. **(b-d)** TEM images* of **(b)** untreated NiP/C, **(c)** bulk NiP/C after 1-minute treatment in 5% $O_2$ atmosphere, and **(d)** bulk NiP/C after 1-minute treatment in Ar atmosphere.

Analysis of the XRD spectrum (**Figure 4 (a)**) of the prepared NiP/C shows that $Ni_2P$ is the bulk phase of the material, indicating a successful synthesis. Less intense signals of $Ni_2P$ at higher diffraction angles are not seen in the sample due to the overwhelming intensity of the carbon support signal (~25°). TEM images reveal larger nanoparticles with a core-shell (NiP-NiO) morphology which is unaffected after plasma treatment. The denser NiP core (darkest) is seen surrounded by a thin, less dense oxide shell (lighter).

**TEM images by Dezhen Wu*

## Electrochemical Evaluation

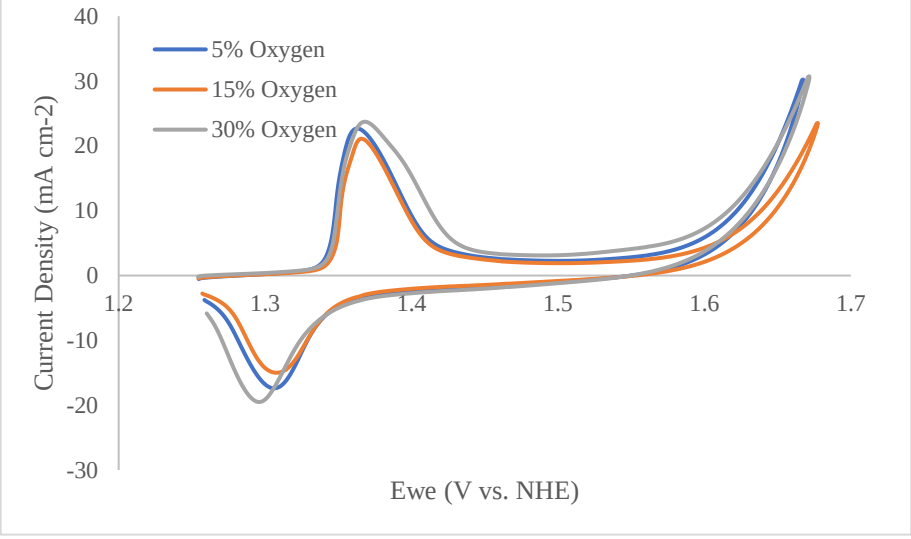


**Figure 5:** Comparison of CV curves between NiP samples treated in plasmas with varying oxygen concentrations.

To identify the percentage of oxygen to use for further time-varying treatments, three samples of as prepared NiP were treated for 5 minutes in plasmas with varying oxygen concentrations. Oxygen was diluted for plasma treatment through flow rate control to 30, 15, and 5% by volume. A CV scan was used to judge the activity of each treated sample. Material treated with 5% and 30% performed similarly according to their CV curves (**Figure 5**), however, after treatment in the more concentrated oxygen plasma environment, a white material was produced separate from the NiP bulk material. The white material was thought to be nickel oxide, a product of nickel sputtering from the bulk material and reacting in the oxygen plasma atmosphere. The mild, 5% oxygen atmosphere was chosen for further evaluation.

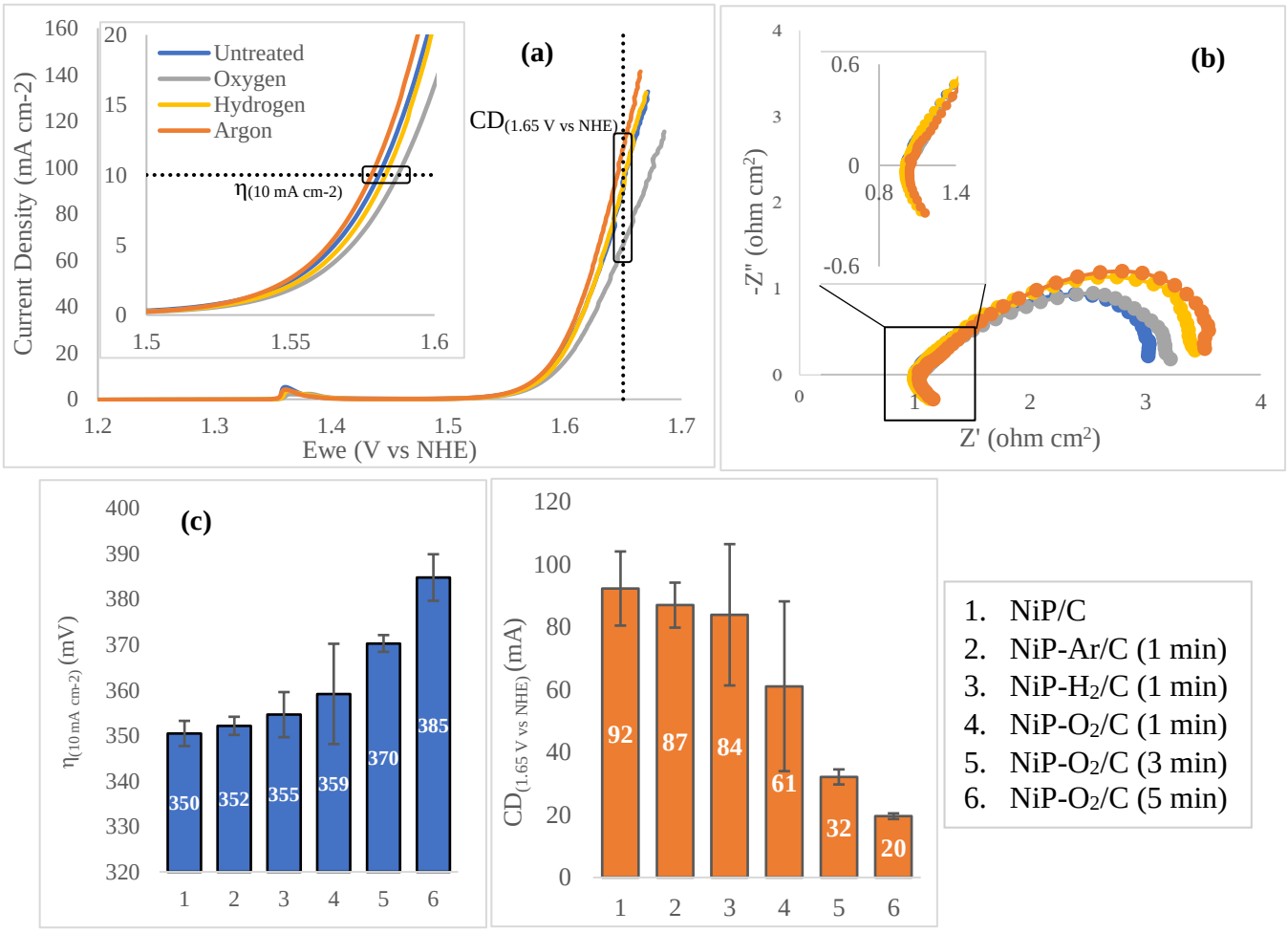


**Figure 6: (a)** Comparison of representative LSV curves for untreated sample and after treatment in different plasma atmospheres for 1-minute. A comparison of the activation region of the LSV curves is shown in the inset. **(b)** Comparison of Nyquist plots (normalized to GCE surface area) between tests of each sample, used for iR potential correction. Inset shows similar real axis intercepts (solution resistances) between tests. **(c)** Comparison of onset overpotential of electrodes and current density at 1.65 V vs NHE. Error bars for 1-minute and untreated samples reflect one standard deviation from triplicate tests, 3- and 5-minute error bars show error between duplicate tests.

The solution resistance measured by EIS for each test was in the range of 5.15-5.35 Ω as shown in **Figure 6 (b)**. Changes in the distance between reference and working electrode in the cell between tests likely account for this range of the measured solution resistance.

Results from the LSV measurement shown in **Figure 6 (a, c)** suggest that electrodes prepared with untreated NiP/C and NiP/C treated with argon and hydrogen plasma for 1 minute

(NiP-Ar/C (1 min) and NiP-$H_2$/C (1 min), respectively) performed similarly with activation overpotentials in the range of η = 350-355 mV and $CD_{(1.65\ V\ vs\ NHE)}$ = 84-92 mA/cm$^2$ at higher overpotentials. The electrode prepared with the oxygen plasma treated sample (NiP-$O_2$/C (1 min)) performed the worst of the one minute samples (η = 359 mV and $CD_{(1.65\ V\ vs\ NHE)}$ = 61 mA/cm$^2$), suggesting that the oxygen plasma environment was too harsh, possibly creating unwanted byproducts during treatment.

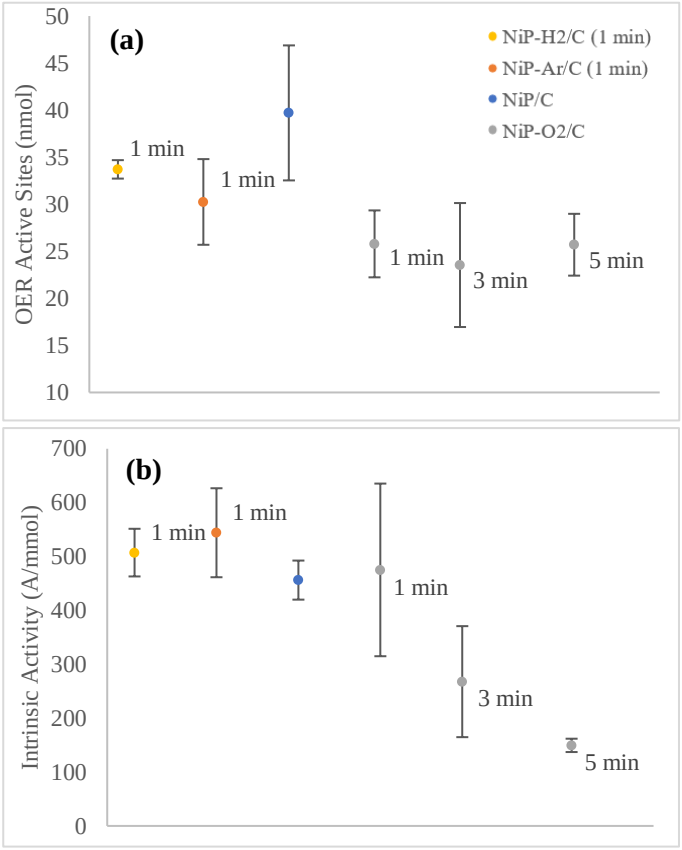


**Figure 7: (a)** Summary of OER active sites measured before and after plasma treatment with various atmospheres and with varying treatment time. **(b)** Summary of intrinsic OER activity on NiP nanoparticles after plasma treatment. Error bars for 1-minute and untreated samples reflect one standard deviation from triplicate tests, 3- and 5-minute error bars show error between duplicate tests.

Current measured at 1.65V ($i_{(1.65\ V\ vs\ NHE)}$) was normalized by the number of active sites, determined from the $Ni^{2+}/Ni^{3+}$ oxidation peak, to yield the intrinsic OER activity of each sample. The comparison of the measured active sites in **Figure 7 (a)** shows overall, that plasma treatment reduces the number of active sites participating in OER by about 30% compared to the untreated sample. Oxygen plasma treated samples show the lowest number of active sites, likely in part due to the sputtering of Ni and reaction to nickel oxide hypothesized to take place during treatment.

Shown in **Figure 7 (b)**, NiP-Ar/C (1 min) had the highest intrinsic OER activity of the evaluated samples at 544 A/mmol. NiP-$H_2$/C (1 min) and NiP-$O_2$/C (1 min) performed slightly better than untreated NiP/C (456 A/mmol), while the samples that underwent extended oxygen treatment (NiP-$O_2$/C (3 min) and NiP-$O_2$/C (5 min)) performed worse. The large error bars on NiP-$O_2$/C (1 min) could be attributed to the presence of varying amounts of nickel oxide in the material as a byproduct of plasma treatment.

## Surface Analysis

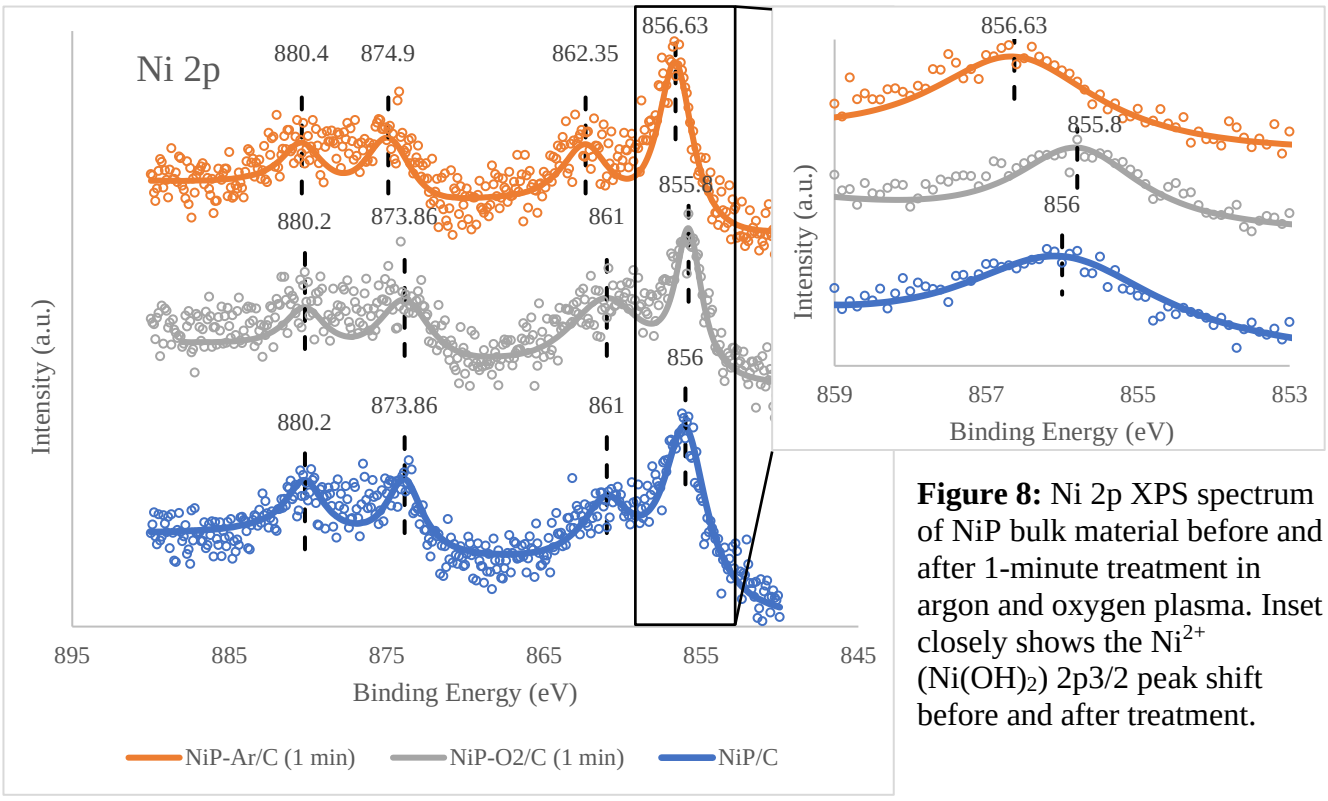


**Figure 8:** Ni 2p XPS spectrum of NiP bulk material before and after 1-minute treatment in argon and oxygen plasma. Inset closely shows the $Ni^{2+}$ ($Ni(OH)_2$) 2p3/2 peak shift before and after treatment.

Ni 2p, P 2p, O 1s, and C 1s XPS spectra were collected for untreated, 1-minute argon, and 1-minute oxygen treated samples for surface analysis and comparison. **Figure 8** shows the Ni 2p spectra for each sample which have been deconvoluted into the solid lines shown. Peaks in the range of 855.8-856.63 eV correspond with the identity of $Ni(OH)_2$ 2p3/2 signals (855.3-856.6 eV).[25] In this range, $Ni^{3+}$ may also provide a signal; the range for $Ni_2O_3$ is reported to be

very narrow between 855.8-856 eV.[25] $Ni^{2+}$ as $NiO/Ni(OH)_2$ provides a 2p1/2 signal at higher binding energies of 871.8-873.8 eV. Peaks at ~861 and ~880 eV correspond to 2p3/2 and 2p1/2 satellite peaks, respectively.

It is difficult to distinctly quantify the ratio of $Ni^{3+}/Ni^{2+}$ from the Ni 2p XPS spectra because of the narrow binding energy range to observe rare $Ni^{3+}$ and the low signal-to-noise ratio of the spectra, however, a significant shift in the Ni 2p3/2 peak binding energy results from plasma treatment. Argon plasma treatment results in a significant peak shift to a higher binding energy suggesting an increased Ni valence, while treatment with oxygen plasma yielded a decreased Ni valence.

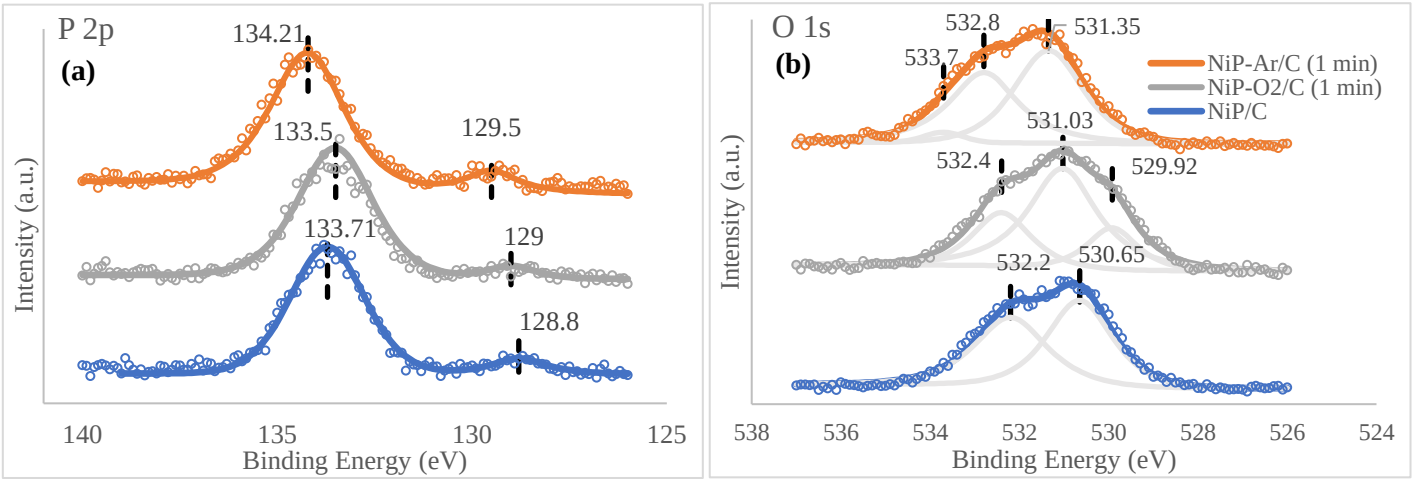


**Figure 9: (a)** comparison of P 2p XPS spectra before and after plasma treatment; **(b)** comparison of O 1s XPS spectra before and after plasma treatment

The P 2p signal (**Figure 9 (a)**) before and after plasma treatment shows the same peak shift trend as the Ni 2p signal, suggesting P has a higher valence after plasma treatment with argon, but lower valence after oxygen plasma treatment. At ~133.5 eV, the higher binding energy peak can be attributed to the P-O bonding nature in phosphates, while the lower binding energy peak at ~129 eV can be attributed to the Ni-P bonding nature in phosphides. The relative

intensity of the phosphide peak is much lower than the phosphate peak as would be expected, as the surface of the nanoparticles may be oxidized to phosphate while the core will remain as NiP.

O 1s spectra were deconvoluted into several peaks which represent various modes of oxygen bonding at the material surface seen in **Figure 9 (b)**. Ni-O bonding in nickel oxides present on the surface of the material likely contributes the peak at 530.65 eV. The second peak at a higher binding energy present in the spectrum of the untreated sample at 532.2 eV could be attributed to oxygen bonding in $Ni(OH)_2$. These two peaks should be present in the spectra of the treated samples, and likely are present, but are shifted to higher binding energies. In the spectrum of the argon treated sample, the third, low-intensity peak present at 533.7 eV may signify the presence of an oxygen bonding mode in which oxygen exists in a higher valence state. The third peak present in the O 1s spectrum of the oxygen treated sample may be contributed from the oxidation of $Ni(OH)_2$ (531.2 eV),[25] with the oxygen bond now having a similar nature to O in NiOOH (528.9 eV).[25]

It should be reiterated that the XPS spectra reported have not been corrected to align the C 1s peak to the binding energy of advantageous carbon (285 eV). There is a strong possibility that the carbon support is charged as a result of plasma treatment, for which a shift in C 1s binding energy would be expected. **Figure 10** shows the shift seen between treated and untreated samples. An anomaly in the oxygen plasma treated C 1s sample is seen where there is a small peak at 282.3 eV.

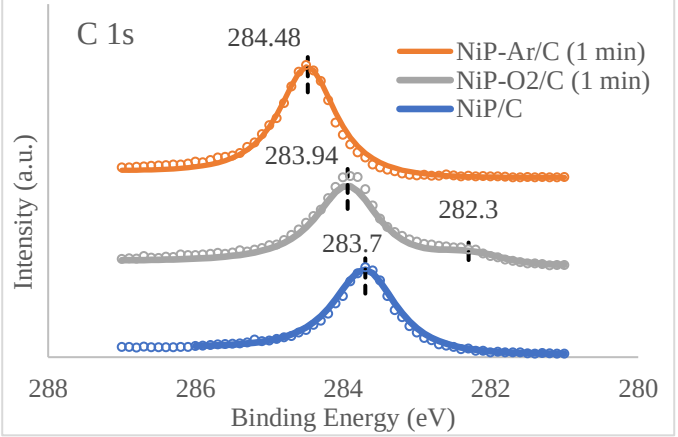


**Figure 10:** Comparison of C 1s spectra collected before and after plasma treatment.

# Conclusion

Plasma treatment remains to be a quick and facile method to manipulate surface properties of bulk materials. In this experiment, plasma treatment was employed to control the valence of OER active metal sites in order to optimize the performance of a supported NiP catalyst. A small improvement in intrinsic activity was seen by treating the material in argon plasma for 1 minute, while treatment in oxygen and hydrogen plasmas either worsened performance or did not yield a very significant improvement in activity. To understand how treatment with plasma changed the valence of elements on the surface of the material, XPS spectra were recorded before and after treatment. No clear correlation between valence state and OER performance could be confidently identified from XPS analysis, but some chemical surface modification was observed as a result of plasma treatment. Further studies may be conducted to treat transition metal phosphide materials synthesized from transition metals with lower redox potentials to observe a correlation more easily between metal valence state and changes in OER activity after treatment.

# References


1. Chu, S.; Majumdar, A. Opportunities and Challenges for a Sustainable Energy Future. *Nature* **2012**, *488* (7411), 294–303. https://doi.org/10.1038/nature11475.
2. Seh, Z. W.; Kibsgaard, J.; Dickens, C. F.; Chorkendorff, I.; Nørskov, J. K.; Jaramillo, T. F. Combining Theory and Experiment in Electrocatalysis: Insights into Materials Design. *Science* **2017**, *355* (6321). https://doi.org/10.1126/science.aad4998.
3. Acar, C.; Dincer, I. Comparative Assessment of Hydrogen Production Methods from Renewable and Non-Renewable Sources. *International Journal of Hydrogen Energy* **2014**, *39* (1), 1–12. https://doi.org/10.1016/j.ijhydene.2013.10.060.
4. Gray, H. Powering the planet with solar fuel. *Nature Chem* **2009**, *1*, 7. https://doi.org/10.1038/nchem.141.
5. Gasteiger, H. A.; Markovic, N. M. Just a Dream or Future Reality? *Science* **2009**, *324* (5923), 48–49. https://doi.org/10.1126/science.1172083.
6. Zeng, K.; Zhang, D. Recent Progress in Alkaline Water Electrolysis for Hydrogen Production and Applications. *Progress in Energy and Combustion Science* **2010**, *36* (3), 307–326. https://doi.org/10.1016/j.pecs.2009.11.002.
7. Tahir, M.; Pan, L.; Idrees, F.; Zhang, X.; Wang, L.; Zou, J. J.; Wang, Z. L. Electrocatalytic Oxygen Evolution Reaction for Energy Conversion and Storage: A Comprehensive Review. *Nano Energy* **2017**, *37*, 136–157. https://doi.org/10.1016/j.nanoen.2017.05.022.
8. Chen, L.; Dong, X.; Wang, Y.; Xia, Y. Separating Hydrogen and Oxygen Evolution in Alkaline Water Electrolysis Using Nickel Hydroxide. *Nature Communications* **2016**, *7* (1), 1–8. https://doi.org/10.1038/ncomms11741.
9. Francàs, L.; Corby, S.; Selim, S.; Lee, D.; Mesa, C. A.; Godin, R.; Pastor, E.; Stephens, I. E. L.; Choi, K. S.; Durrant, J. R. Spectroelectrochemical Study of Water Oxidation on Nickel and Iron Oxyhydroxide Electrocatalysts. *Nature Communications* **2019**, *10* (1), 1–10. https://doi.org/10.1038/s41467-019-13061-0.
10. Jin, S. Are Metal Chalcogenides, Nitrides, and Phosphides Oxygen Evolution Catalysts or Bifunctional Catalysts? *ACS Energy Letters* **2017**, *2* (8), 1937–1938. https://doi.org/10.1021/acsenergylett.7b00679.
11. Sapountzi, F. M.; Gracia, J. M.; Weststrate, C. J. (Kees J.; Fredriksson, H. O. A.; Niemantsverdriet, J. W. (Hans). Electrocatalysts for the Generation of Hydrogen, Oxygen and Synthesis Gas. *Progress in Energy and Combustion Science* **2017**, *58*, 1–35. https://doi.org/10.1016/j.pecs.2016.09.001.
12. Yuan, N.; Jiang, Q.; Li, J.; Tang, J. A Review on Non-Noble Metal Based Electrocatalysis for the Oxygen Evolution Reaction. *Arabian Journal of Chemistry* **2020**, *13* (2), 4294–4309. https://doi.org/10.1016/j.arabjc.2019.08.006.
13. Liu, K.; Zhang, C.; Sun, Y.; Zhang, G.; Shen, X.; Zou, F.; Zhang, H.; Wu, Z.; Wegener, E. C.; Taubert, C. J.; Miller, J. T.; Peng, Z.; Zhu, Y. High-Performance Transition Metal Phosphide Alloy Catalyst for Oxygen Evolution Reaction. *ACS Nano* **2018**, *12* (1), 158-167. https://doi.org/10.1021/acsnano.7b04646.
14. Cheng, J.; Yang, J.; Kitano, S.; Juhasz, G.; Higashi, M.; Sadakiyo, M.; Kato, K.; Yoshioka, S.; Sugiyama, T.; Yamauchi, M.; Nakashima, N. Impact of Ir-Valence Control and Surface Nanostructure on Oxygen Evolution Reaction over a Highly Efficient Ir-

TiO2 Nanorod Catalyst. *ACS Catalysis* **2019**, *9* (8), 6974–6986. https://doi.org/10.1021/acscatal.9b01438.
15. Zhang, B.; Wang, L.; Cao, Z.; Kozlov, S. M.; Pelayo García de Arquer, F.; Thang Dinh, C.; Li, J.; Wang, Z.; Zheng, X.; Zhang, L.; Wen, Y.; Voznyy, O.; Comin, R.; De Luna, P.; Regier, T.; Bi, W.; Ercan Alp, E.; Pao, C.-W.; Zheng, L.; Hu, Y.; Ji, Y.; Li, Y.; Zhang, Y.; Cavallo, L.; Peng, H.; Sargent, E. H. High-Valence Metals Improve Oxygen Evolution Reaction Performance by Modulating 3d Metal Oxidation Cycle Energetics. *Nature Catalysis* **2020**, *3*, 985-992. https://doi.org/10.1038/s41929-020-00525-6.
16. Zhao, C.; Li, N.; Zhang, R.; Zhu, Z.; Lin, J.; Zhang, K.; Zhao, C. Surface Reconstruction of La 0.8 Sr 0.2 Co 0.8 Fe 0.2 O 3−δ for Superimposed OER Performance. *ACS Appl Mater Interfaces* **2019**, *11* (51), 47858-47867. https://doi.org/10.1021/acsami.9b13834.
17. Chen, G.; Zhou, W.; Guan, D.; Sunarso, J.; Zhu, Y.; Hu, X.; Zhang, W.; Shao, Z. Two Orders of Magnitude Enhancement in Oxygen Evolution Reactivity on Amorphous Ba0.5Sr0.5Co0.8Fe0.2O3−d Nanofilms with Tunable Oxidation State. *Science Advances* **2017**, *3* (6), 1603206–1603206. https://doi.org/10.1126/sciadv.1603206.
18. You, B.; Jiang, N.; Sheng, M.; Bhushan, M. W.; Sun, Y. Hierarchically Porous Urchin-Like Ni 2 P Superstructures Supported on Nickel Foam as Efficient Bifunctional Electrocatalysts for Overall Water Splitting. *ACS Catalysis* **2016**, *6* (2), 714-721. https://doi.org/10.1021/acscatal.5b02193.
19. Wang, Z.; Zhang, Y.; Neyts, E. C.; Cao, X.; Zhang, X.; W-L Jang, B.; Liu, C. Catalyst Preparation with Plasmas: How Does It Work? *ACS Catalysis* **2018**, *8* (3), 2093-2110. https://doi.org/10.1021/acscatal.7b03723.
20. Tyczkowski, J. Cold Plasma Produced Catalytic Materials. In *Plasma Science and Technology - Progress in Physical States and Chemical Reactions*; InTech **2016**, 25-65. https://doi.org/10.5772/61832.
21. Witvrouwen, T.; Paulussen, S.; Sels, B. The Use of Non-Equilibrium Plasmas for the Synthesis of Heterogeneous Catalysts. *Plasma Processes and Polymers* **2012**, *9* (8), 750–760. https://doi.org/10.1002/ppap.201200004.
22. Wirth, S.; Harnisch, F.; Quade, A.; Brüser, M.; Brüser, V.; Schröder, U.; Savastenko, N. A. Enhanced Activity of Non-Noble Metal Electrocatalysts for the Oxygen Reduction Reaction Using Low Temperature Plasma Treatment. *Plasma Processes and Polymers* **2011**, *8* (10), 914–922. https://doi.org/10.1002/ppap.201100020.
23. Guan, Q.; Li, W.; Zhang, M.; Tao, K. Alternative Synthesis of Bulk and Supported Nickel Phosphide from the Thermal Decomposition of Hypophosphites. *Journal of Catalysis* **2009**, *263* (1), 1–3. https://doi.org/10.1016/j.jcat.2009.02.008.
24. Greczynski, G.; Hultman, L. Compromising Science by Ignorant Instrument Calibration-Need to Revisit Half a Century of Published XPS Data. *Angewandte Chemie International Edition* **2020**, *59* (13), 5002-5006. https://doi.org/10.1002/anie.201916000.
25. NIST X-ray Photoelectron Spectroscopy Database, NIST Standard Reference Database Number 20, National Institute of Standards and Technology, Gaithersburg MD, 20899 (2000), http://dx.doi.org/10.18434/T4T88K, (retrieved 12 Apr. 2021)